Reactive momentum transfer contributes to the self propulsion of Janus particles

Reactive momentum transfer contributes to the self propulsion of Janus particles

Shaltiel Eloul,[1] Wilson C K Poon,[2] Oded Farago,[1,3] and Daan Frenkel[1]

[1]*Department of Chemistry, University of Cambridge, Lensfield Road, Cambridge CB2 1EW, United Kingdom*

[2]*SUPA and School of Physics and Astronomy, The University of Edinburgh, Peter Guthrie Tait Road, Edinburgh EH9 3FD, United Kingdom*

[3]*Biomedical Engineering Department, Ben Gurion University, Be'er Sheva 84105, Israel*

(Dated: April 6, 2020)

Abstract

We report simulations of a spherical Janus particle undergoing exothermic surface reactions around one pole only. Our model excludes self-phoretic transport by design. Nevertheless, net motion occurs from direct momentum transfer between solvent and colloid, with speed scaling as the square root of the energy released during the reaction. We find that such propulsion is dominated by the system's short-time response, when neither the time dependence of the flow around the colloid nor the solvent compressibility can be ignored. Our simulations agree reasonably well with previous experiments.

Self-propelled, or active, colloids display novel phenomena such as non-monotonic density-dependent viscosity and swarming [1, 2]. The field has benefitted from the invention of synthetic micro-swimmers [3]. Golestanian et al. suggested that asymmetric chemical reactions on the surface of a sphere could generate a corresponding asymmetric distribution of molecular moities; the resulting concentration gradient should propel the particle by diffusiophoresis [4]. Janus polystyrene colloids half coated with platinum [5] were thought to offer a paradigmatic example; however, salt and pH dependence pointed instead to self-electrophoresis [6–8]. Self-thermophoretic propulsion is considered unlikely (but see [9]); however, concentration gradients around an asymmetrically laser-heated particle in a near-critical binary mixture can propel micro-swimmers [10]. The idea of non-phoretic propulsion by osmotic pressure gradients is less accepted [11, 12], but bubble-driven propulsion of macroscopic swimmers [13, 14] is well established, and surface flows may propel emulsion droplets [15]. At a more microscopic level, Felderhof [16] has considered the propulsion of a Janus particle due to the flow field caused by a sudden localized volume expansion in the fluid.

Strikingly, many phoretic micro-swimmers are propelled by decomposing high specific impulse rocket monopropellants, principally hydrogen peroxide and hydrazine [17]. Interestingly, the 'detonation' of energetic molecules on a particle surface generates an impulse directly, but this has not yet been explored as a potential propulsive mechanism.

We demonstrate the viability of such 'rocket propulsion' by mesoscopic simulations of an exothermic surface reaction that transfers momentum between solvent and colloid (while conserving momentum), which causes a net displacement of the colloid. A finite reaction rate then results in a relative motion of the colloid with respect to the solvent, at a speed we estimate to be non-negligible compared to self-phoretic propulsion using H_2O_2 as fuel.

Net colloidal propulsion that is not driven by the formation of a persistent (micro)bubble is hydrodynamically unobvious. Intuitively, since the system momentum is conserved, impulsive transfer to the colloid is almost instantly cancelled by a counter-flow, dissipating energy but giving no directional movement. But this neglects the finite time $\sim R^2/\nu$ for transverse momentum to diffuse away from a colloid of radius R in a fluid of kinematic viscosity ν. Moreover, a third of the momentum transferred to a compressible fluid is transported away as sound [18] and so cannot contribute to the local, retarding flow. Therefore, the effect of an impulsive surface force is neither cancelled immediately nor locally by hydrodynamic drag forces.

To model impulsive transport, we use dissipative particle dynamics (DPD) [19, 20], which conserves momentum and thus provides a realistic description of compressible hydrodynamics. The colloid-fluid interaction has been chosen to give negligible excess enthalpy or density of the fluid particles near the colloid. Hence, by design, self-phoretic transport should be negligible. We allow exothermic reactions at the colloid-fluid interface, resulting in a local pressure spike at the colloid's surface.

The force on DPD fluid particle i is given by $\mathbf{f_i} = \sum_{\mathbf{j}\neq\mathbf{i}} (\mathbf{F^C_{ij}} + \mathbf{F^D_{ij}} + \mathbf{F^R_{ij}})$, where $\mathbf{F^{C,D,R}}$ are, respectively, conservative, dissipative and random pair forces with particle j. For convenience, we assume that the potential energy of interaction between two fluid particles is given by a soft quadratic effective potential, resulting in a conservative pair force $\mathbf{F^C_{ij}} = \alpha(1 - r_{ij}/r_c)\hat{\mathbf{r}}_{\mathbf{ij}}$ where r_{ij} denotes the distance $|\mathbf{r_i} - \mathbf{r_j}|$ and $\hat{\mathbf{r}}_{\mathbf{ij}} = (\mathbf{r_i} - \mathbf{r_j})/r_{ij}$ is the corresponding unit vector. The constant α sets the repulsion strength and mimics the compressibility of water [20]. The dissipative and random forces connect via fluctuation-dissipation relations [21]: $\mathbf{F^D_{ij}} = -\gamma\omega(r_{ij})(\mathbf{v_{ij}} \cdot \hat{\mathbf{r}}_{\mathbf{ij}})\hat{\mathbf{r}}_{\mathbf{ij}}$ and $\mathbf{F^R_{ij}} = \sqrt{2\gamma kT\omega(r_{ij})}\frac{dW_{ij}}{dt}\hat{\mathbf{r}}_{\mathbf{ij}}$, where $\mathbf{v_{ij}} = (\mathbf{v_i} - \mathbf{v_j})$ is the relative velocity, γ is the friction coefficient controlling energy dissipation into the fluid, and W_{ij} is a Wiener process: $\int_0^{\Delta t} dW_{ij} = \sqrt{\Delta t}\zeta_{ij}$, where ζ_{ij} is a standard Gaussian random number. The weight function $\omega(r)$ takes the form $\omega(r_{ij}) = (1 - r_{ij}/r_c)^2$.

Table I summarises our units and parameters. A few comments are in order. Our DPD particle has mass m_f corresponding to three average solvent molecules. As we aim to describe a typical 10 wt.% H_2O_2 solution used in experiments, the average mass of a DPD particle is 59.4 (in atomic units). To reproduce the mass density of this solution, $1040\,\mathrm{kg\,m^{-3}}$ [22], we use a DPD density of $\rho r_c^3 = 3.0$. To reproduce the compressibility of water at room temperature, $\alpha = 25$ and $\gamma = 4.5$ [20]. Using [20], we estimate a shear viscosity of $\eta = 0.96$

TABLE I. Simulation units, parameters and time scales

Quantity	DPD units	Physical units
Mass	Fluid particle mass $m_f = 1$	9.76×10^{-26} kg
Length	Cut off distance $r_c = 1$	6.56 Å
Energy	Thermal energy $\epsilon = k_B T = 1$	4.11×10^{-21} J
Speed	$(k_B T/m_f)^{0.5} = 1$	$205.2\,\mathrm{m\,s^{-1}}$
Time	$\tau = r_c(k_B T/m_f)^{-0.5} = 1$	3.2 ps
Viscosity	$\eta_0 = (\epsilon/r_c^3)\tau = 1$	0.047 mPa s
Parameter	Value	
ρ, α, γ	3.0, 25.0, 4.5	
Time scale	Value	
$R(=1.36)/c_s$	0.35[a]	
$\tau^S = m/\lambda$	1.2	
$R(=1.36)^2/\nu$	6.4	
Dimensionless speed properties[b]	Value	
Ma	$10^{-3} - 10^{-2}$	Mach number
Re	~ 0.5	Reynolds number
Pe	~ 0.5	Péclet number

[a] Sound speed $c_s = \sqrt{\mathrm{d}p/\mathrm{d}\rho} \approx 4$ from the equation of state [20].

[b] The fluid speed properties are for the calculated range of colloid sizes and resulting speeds in this work.

in DPD units, corresponding to 4.7×10^{-5} Pa s, about 5% that of water; we correct for this when comparing with experiments. The fluid equations of motion were integrated using the modified velocity-Verlet algorithm [20] with a reduced time step of 5×10^{-3}.

We model the Janus colloid using a dense spherical layer of 'frozen' DPD particles, Fig. 1a. Its radius R ($= 2.3 \equiv 1.5$ nm unless otherwise stated) is defined as the distance between the center of the colloid and the centers of the surface particles. Our surface-particle density is high enough to suppress penetration of fluid particles during the simulation. For surface densities $\rho_s \gtrsim 25$, the speed of the reaction-driven colloid was insensitive to ρ_s. With enough fluid particles around the colloid, it is sufficient not to include dissipative and random forces

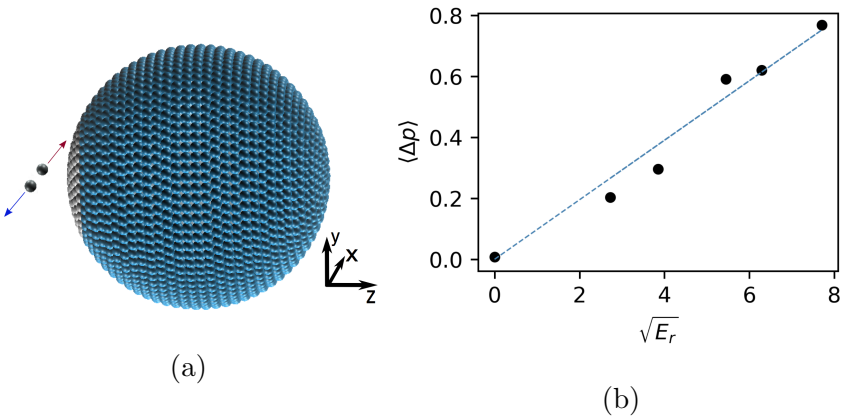

(a) (b)

FIG. 1. (a) An active colloid densely covered with "frozen" DPD particles. A pair of solvent particles (black) in the vicinity of the active zone (grey) experiences a change of their velocities according to Eqn 1 at the time of reaction. (b) Average momentum transferred to the colloid from the fluid as function of square root of energy release. The line is a linear fit.

between the 'frozen' surface particles and fluid particles, and take this interaction as repulsive only. This has minimal effect on the hydrodynamic boundary conditions (the colloid surface is still fairly rough) and does not change our conclusions qualitatively. Since the fluid particles interact with the colloid through conservative forces, the colloid acquires the temperature of the DPD fluid in the absence of chemical reactions. We freeze out the rotational motion of the colloid, which only acts on longer time scales. This is sufficient for particle speeds of $\sim 1\,\mu\mathrm{m\,s}^{-1}$ in sub-micro ($\sim 100\,\mathrm{nm}$) to micro Janus particles as rotational diffusion $\sim R^{-3}$. The total force on the center-of-mass of the colloid is the sum of all (repulsive) forces between the frozen particles on its surface and the neighbouring fluid particles. The colloidal equations of motion were also solved using the velocity-Verlet algorithm.

We chose parameters appropriate for the reaction $2\,H_2O_2 \longrightarrow O_2 + 2\,H_2O$ on a Pt surface with standard enthalpy $\Delta H^{\ominus} = 1.017\,\mathrm{eV} \equiv 39.6 k_B T$ at room temperature. A reaction is modelled by increasing the kinetic energy of a pair of neighboring DPD particles close to the catalytic surface by $\Delta H^{\ominus}$, conserving momentum and leaving all species unchanged. For simplicity but without loss of generality, we constrain the active zone for reactions to a small area on the particle surface (grey patch in Fig. 1a). Reactions occur at a rate, or frequency, f (in inverse time units).

The DPD thermostat acts as a local energy sink and reduces the efficiency of momentum

transfer due to reaction. For comparison, in a simulation without frictional forces, the speed of the colloid increased by a factor of ~ 2.2. The thermostat simply suppresses heating of the fluid and minimises possible temperature gradients along the colloidal surface (see also Supplementary Information (SI)), which in any case is probably less important as (by design) our excess surface enthalpy (and hence any thermophoresis) is minimized. Diffusiophoresis can also be ignored because (again by design) the reactants and products are identical and so have the same interaction with the colloidal surface.

The energy release during an individual hydrolysis reaction event at time t^* is modelled by instantaneously increasing the kinetic energy of a pair of neighboring DPD particles close to the catalytic surface by $\Delta H^{\ominus}$, conserving momentum and leaving all species unchanged. Energy and momentum conservation then leads to:

$$\Delta \mathbf{v}^2 + \Delta \mathbf{v} \cdot (\mathbf{v_a} - \mathbf{v_b}) = \frac{E_r}{m_f}. \tag{1}$$

where $\mathbf{v_a}$ and $\mathbf{v_b}$ are the particle velocities before the reaction, which are changed by $\pm\Delta\mathbf{v}$ due to energy injection. The direction of $\Delta\mathbf{v}$ is randomly chosen from a uniform distribution, with magnitude from Eqn 1.

We measure an average net momentum transfer to the colloid as a result of near-surface reactions, $\langle \Delta p \rangle$, which scales as $E_r^{0.5}$, Fig. 1b, as expected on dimensional grounds for 'rocket propulsion'. This scaling rules out self-thermophoresis, for which $\langle \Delta p \rangle \sim E_r$, and self-diffusiophoresis, for which $\langle \Delta p \rangle \sim E_r^0$. Only a fraction of $\Delta H^{\ominus}$ is converted into momentum of the colloid. The precise fraction depends on details, including the model parameters that determine friction. In addition, for real catalytic surfaces, part of the reaction energy will go into the colloid - how much depends on the microscopic details of the reaction. and the surface morphology. However, it is plausible to assume that a fair fraction of the reaction energy (tens of percents) will power the momentum transfer between colloid and solvent. Detailed atomistic simulations would be needed to arrive at a quantitative estimate.

The finite momentum transfer imparts a net transient velocity to the colloid along its polar, or z, axis, which points directly away from the active patch. Figure 2 (black line) shows the colloidal velocity as a function of $t - t^*$, the time interval since the moment (t^*) when the reaction energy was released to the fluid. $\langle v_z \rangle$ was obtained by averaging over 10^4 independent reaction events. For the reaction rate used ($f = 0.04$), the effects of successive reaction events are uncorrelated.

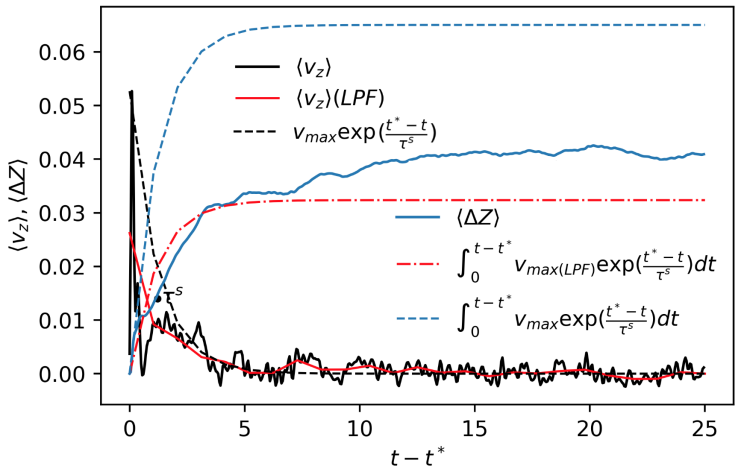

FIG. 2. A transient profile of the velocity (black curve) and the total displacement (blue curve) of an active colloid ($R = 1.36$) as function of time (t) from the time of reaction (t^*). The velocity decay and the total displacement after the reaction impulse are compared to Stokes friction (black dashed curve) and its time integral (blue dashed curve).The red curve shows the result of low pass filtering (LPF).

At short times, $v(t - t^*)$ shows strong oscillations because the fluid is compressible. However, these oscillations do not appear to contribute to the particle displacement, i.e. the time integral of v. We average out such short-time non-monotonicity as well as the noise using a low-pass filter to give $\langle v_z \rangle$(LPF) (red line). Neither the raw nor the low-pass filtered data follow the single exponential (black dashed) from an initial $\langle v_0 \rangle$ predicted by Stokes Law:

$$\langle v_z \rangle = \langle v_0 \rangle \exp\left[-\left(\frac{t - t^*}{\tau^S}\right)\right], \tag{2}$$

where $\tau^S = m/\lambda \approx 1.2$ (with λ the Stokes drag coefficient). The actual decay of $\langle v_z \rangle$ is substantially faster, because our 'detonation' *ansatz* generates a force *dipole* rather than a monopole in the fluid.

Integrating the average transient velocity gives the average displacement of the colloid in response to a reaction event, $\langle \Delta z \rangle$, Fig. 2 (blue line). There is a rapid rise at short times. One might expect that this rapid rise should saturate beyond $t - t^* \lesssim R^2/\nu \approx 6.4$. This is indeed what we see for the displacement from integrating the smoothed data (red dot-dashed). The rise in the actual displacement (blue) does slow down around this time, but continues to rise to saturate at a value that is about a third higher. This may be related

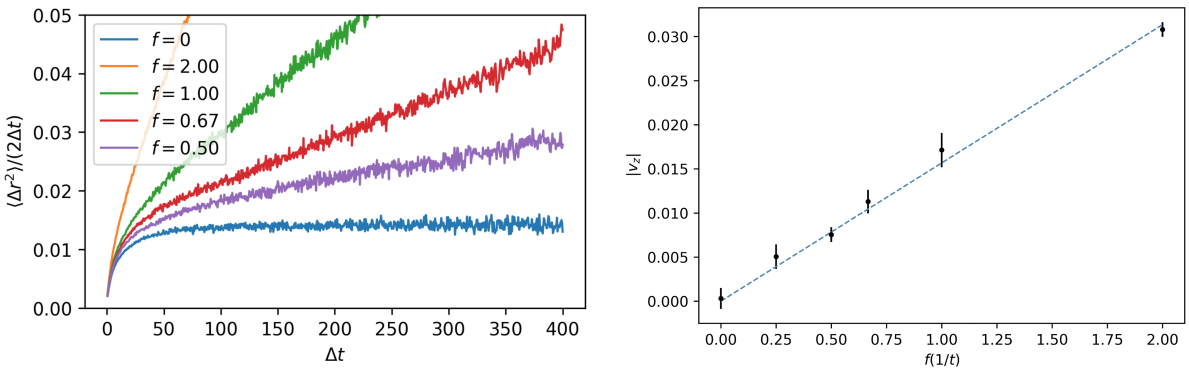

(a) (b)

FIG. 3. (a) $\langle \Delta r^2 \rangle / 2\Delta t$ as function of Δt for various reaction freq"". (b) Drift velocity in z direction as function of reaction frequency (linear fit shown as dashed line). The average velocity and the standard deviations are extracted from total of 15,000 reactions. In both parts, $E_r = 39.6 k_B T$.

to the 'long-time tail' in the velocity autocorrelation function, although our statistics are not good enough to quantify this effect. (Note that the long-time tail in our system will not follow $t^{-3/2}$ scaling because, once again, the chemical reaction results in a force dipole.)

Figure 3 shows the accumulated mean-squared displacement, $\langle \Delta r^2 \rangle$, of the colloid due to a succession of chemical reactions as a function of the elapsed time, Δt, at different reaction frequencies, f. For $f = 0$, $\langle \Delta r^2 \rangle / 2\Delta t$ approaches the Stokes-Einstein diffusivity at long times (see SI). At all $f > 0$, however, $\langle \Delta r^2 \rangle / 2\Delta t$ no longer saturates with time, but asymptotes to a linear regime, indicative of ballistic motion at a constant drift speed.

We verified that the reaction causes no drift in the x and y directions. This average drift speed along the z, or polar, axis of the colloid, $|v_z|$, increases linearly with f, Fig. 3b. Thus, the effects of successive reaction events are simply additive, and $|v_z|$ can be related to the average momentum transfer per reaction $\langle \Delta p \rangle$, the reaction frequency f and the hydrodynamic friction coefficient λ of the colloid by

$$|v_z| = \frac{\langle \Delta p \rangle}{\lambda} f = \left(\frac{\langle \Delta p \rangle}{6\pi\eta} \right) \frac{f}{R}. \tag{3}$$

With the assumption that Stokes friction determines the drag on the Janus particle and that the reaction mechanism is size independent, we can directly map the reaction rates density in our simulation (10^{24}-$10^{27}\,\mathrm{m}^{-2}\,\mathrm{s}^{-1}$) to the (lower) reaction rates density in experiments (order of $10^{22}\,\mathrm{m}^{-2}\,\mathrm{s}^{-1}$).

The second equality, which follows from $\lambda = 6\pi\eta R$, predicts $|v_z| \propto R^{-1}$, which is indeed the case to within the statistical error, for simulations over the range $1.36 \leq R \leq 4.6$ at constant f (where the ratio of the colloidal radius to the box diameter is kept approximately constant) (see SI). The fact that $|v_z| \propto R^{-1}$ implies that $\langle \Delta p \rangle$ (the average momentum transferred to the colloid) is independent of the the colloidal radius. Moreover, λv_z, the average momentum transfer per unit time, is effectively independent of R over this range of radii (see Fig. SI-4) .

We now compare the prediction of Eqn 3 to experiments [6] for a 2 µm-diameter Janus particle half coated with Platinum in 10 wt.% aqueous H_2O_2 with a measured reaction rate of $8 \times 10^{10}\,\mathrm{s}^{-1}$, or $R = 1524$ and $f = 0.24$ in DPD units (cf. Table I). The linear fits in Fig. 3b (and Fig. SI-4) with the DPD viscosity $\eta = 0.96$ give, via Eqn 3, the momentum transfer per reaction, $\langle \Delta p \rangle = 0.62$, which, as we have seen, is nearly R-independent in our simulation range. We extrapolate this to larger radii. Additionally, the reaction is confined to a small area around one pole in our simulations, Fig. 1a. A hemispherical coating will reduce the effective momentum transfer by a factor of two, giving $\langle \Delta p \rangle = 0.31$ for Janus particles. We therefore predict a drift speed of 2.64×10^{-6} in DPD units. This is an overestimate, because the viscosity of our DPD fluid is 20 times lower than that of water, so that we finally predict a drift speed of 1.32×10^{-7} in DPD units, or $\approx 27\,\mu\mathrm{m\,s}^{-1}$.

This is more than twice the observed value of $11 \pm 6\,\mu\mathrm{m\,s}^{-1}$ [6]. Nevertheless, the good order of magnitude agreement suggests strongly that the impulsive propulsion mechanism cannot be ruled out, especially because it is a direct manifestation of momentum conservation, and so cannot be 'designed out' in the way that we have removed diffusiophoresis and thermophoresis in our simulations. That our prediction is off by a numerical factor simply reflects the crudeness of our model. However, that we have an *over*estimate merits further investigation.

Our 'detonation *ansatz*' assumes that the direction of the relative motion of reaction products is randomly distributed relative to the particle surface. However, if we constrain the initial motion of the reaction products to the xz or xy plane (cf. Fig. 1), the resulting z-drift velocity is reduced, and may even change sign (see Fig. SI-5). Adsorption of reactant molecules on the catalytic surface in different orientations may impose such constraints, reducing the drift speed. Moreover, real coatings are rough, so that reactions may occur in solvent trapped in pockets. Indeed, a thought experiment in which reaction occur en-

tirely within a spherical pocket inside the colloid, the net average momentum transfer will be zero, suggesting a possible test of our model. Some particle geometries (e.g. oblate ellipsoids with a small, polar reactive patch) should favour the impulsive propulsion mechanisms over diffusio/thermo-phoresis, making it possible to disentangle phoretic and impulsive propulsion.

Further experimental confrontation is suggested by the near-R-independence of $\langle \Delta p \rangle$. In a system where the reaction on the colloid surface is diffusion controlled, we expect $f \propto R$, and Eqn 3 predicts that $|v_z|$ should be independent of radius. On the other hand, if the reaction is rate limited, $f \propto R^2$, so that $|v_z| \propto R$. For our geometry with surface reactions, Felderhof's model [16] predicts that the colloidal displacement due to a persistent localised volume change scales as $1/R^2$. However, in our model with a fixed number of particles, we do not expect a persistent volume change. Experiments are needed to distinguish our scenario from Felderhof's [16].

In sum, we find that energy release during an exothermic reaction can propel a colloid due to impulsive momentum transfer, which can never be 'turned off' in experimental systems of this kind. Our model is undoubtedly over-simplified and there are many other factors that may affect the efficiency of momentum transfer between solvent and colloid, such as the details of catalytic decomposition and surface topography. Nevertheless, we find the magnitude of speeds attainable means that this mechanism can seldom, if ever, be ignored as one of the propulsion mechanisms of real-life micron-sized Janus particles in which phoretic mechanisms also operate.

The Cambridge work was partially funded by the Horizon 2020 program through 766972-FET-OPEN-NANOPHLOW. WCKP was funded by ERC Advanced Grant ERC-2013-AdG 340877-PHYSAP. We thank Alexander Morozov, Peter Wolynes and Ubbo Felderhof for enlightening discussions.

[1] V. A. Martinez, E. Clément, J. Arlt, C. Douarche, A. Dawson, J. Schwarz-Linek, A. K. Creppy, V. Škultéty, A. N. Morozov, H. Auradou, and W. C. K. Poon, A combined rheometry and imaging study of viscosity reduction in bacterial suspensions, Proceedings of the National Academy of Sciences **117**, 2326 (2020).

[2] W. C. K. Poon, From *Clarkia* to *Escherichia* and Janus: The physics of natural and synthetic active colloids, in *Physics of Complex Colloids*, edited by C. Bechinger, F. Sciortino, and P. Ziherl (Società Italiana di Fisica, Bologna, 2013) pp. 317–386.

[3] S. J. Ebbens and J. R. Howse, In pursuit of propulsion at the nanoscale, Soft Matter **6**, 726 (2010).

[4] R. Golestanian, T. Liverpool, and A. Ajdari, Propulsion of a molecular machine by asymmetric distribution of reaction products, Phys. Rev. Lett. **94**, 220801 (2005).

[5] J. Howse, R. Jones, A. Ryan, T. Gough, R. Vafabakhsh, and R. Golestanian, Self-motile colloidal particles: From directed propulsion to random walk, Phys. Rev. Lett. **99**, 048102 (2007).

[6] A. Brown and W. Poon, Ionic effects in self-propelled Pt-coated Janus swimmers, Soft Matter **10**, 4016 (2014).

[7] S. Ebbens, D. Gregory, G. Dunderdale, J. Howse, Y. Ibrahim, T. Liverpool, and R. Golestanian, Electrokinetic effects in catalytic platinum-insulator Janus swimmers, EPL **106**, 58003 (2014).

[8] W. F. Paxton, K. C. Kistler, C. C. Olmeda, A. Sen, S. K. St. Angelo, Y. Cao, T. E. Mallouk, P. E. Lammert, and V. H. Crespi, Catalytic nanomotors: Autonomous movement of striped nanorods, J. Am Chem. Soc. **126**, 13424 (2004).

[9] P. de Buyl and R. Kapral, Phoretic self-propulsion: a mesoscopic description of reaction dynamics that powers motion, Nanoscale **5**, 1337 (2013).

[10] I. Buttinoni, G. Volpe, F. Kümmel, G. Volpe, and C. Bechinger, Active Brownian motion tunable by light, J. Phys. Condens. Matter **24**, 284129 (2012).

[11] J. F. Brady, Particle motion driven by solute gradients with application to autonomous motion: continuum and colloidal perspectives, J. Fluid Mech. **667**, 216 (2011).

[12] F. Jülicher and J. Prost, Generic theory of colloidal transport, Eur. Phys. J. E **29**, 27 (2009).

[13] S. Wang and N. Wu, Selecting the swimming mechanisms of colloidal particles: bubble propulsion versus self-diffusiophoresis, Langmuir **30**, 3477 (2014).

[14] J. Zhang, X. Zheng, H. Cui, and Z. Silber-Li, The self-propulsion of the spherical Pt–SiO_2 Janus micro-motor, Micromachines **8**, 123 (2017).

[15] S. Herminghaus, C. C. Maass, C. Krüger, S. Thutupalli, L. Goehring, and C. Bahr, Interfacial mechanisms in active emulsions, Soft Matter **10**, 7008 (2014).

[16] B. U. Felderhof, Dynamics of pressure propulsion of a sphere in a viscous compressible fluid, J. Chem Phys. **133**, 10.1063/1.3473070 (2010).

[17] "Rocket Propellants", in *Van Nostrand's Encyclopedia of Science, Volume 1*, edited by G. D. Considine and P. H. Kulik (Wiley-Interscience, 2008) 10th ed., pp. 4545–4548.

[18] B. Cichocki and B. Felderhof, Long-time tails in the solid-body motion of a sphere immersed in a suspension, Physical Review E **62**, 5383 (2000).

[19] P. Hoogerbrugge and J. Koelman, Simulating microscopic hydrodynamic phenomena with dissipative particle dynamics, EPL **19**, 155 (1992).

[20] R. D. Groot and P. B. Warren, Dissipative particle dynamics: Bridging the gap between atomistic and mesoscopic simulation, J. Chem. Phys. **107**, 4423 (1997).

[21] P. Espanol and P. B. Warren, Statistical mechanics of dissipative particle dynamics, EPL **30**, 191 (1995).

[22] M. Easton, A. Mitchell, and W. Wynne-Jones, The behaviour of mixtures of hydrogen peroxide and water, Trans. Faraday Soc. **48**, 796 (1952).

Supporting Information: Reactive momentum transfer contributes to the self propulsion of Janus particles

S. Eloul, W.C.K. Poon, O. Farago and D. Frenkel

Passive colloid: To validate our model, we first simulated the Brownian diffusion of a passive colloid in the DPD fluid with periodic boundary conditions. This allows us to estimate the effective hydrodynamic radius of the colloid.

Due to hydrodynamic interactions, the diffusion coefficient of a colloidal particle depends strongly on the size of the periodic box, L. To account for this finite-size effect, we carried out simulations with various periodic box sizes and also, to check consistency, simulations of colloids with different radii in a fixed periodic box. In these simulations we measured the mean squared displacement (MSD) of the colloid in the fluid. For sufficiently long times t, the MSD, $\langle \Delta r^2 \rangle = \langle [r(t+\Delta t) - r(t)]^2 \rangle$ approaches $6D\Delta t$, where D is the colloid diffusion coefficient. This is demonstrated in Fig. 1a and b, showing the MSD as a function of the time from simulations of a particle of radius $R = 2.3$ (corresponding to 1.5nm in physical units) and $L = 7.5R$. We estimate D from

$$D = \left. \frac{\langle \Delta r^2 \rangle}{6\Delta t} \right|_{\Delta t \to \infty}.$$

The MSD analysis exhibits a typical transition from ballistic to diffusive behaviour. A comparison with the Stokes-Einstein relation is also provided in Fig. 2a, showing that D scales inversely with R. We stress that as we do not impose non-slip boundary conditions in the simulations, the diffusion coefficient of the colloid is expected to be higher than the non-slip limit ($D^{\infty} = \frac{kT}{6\pi\eta R}$). To allow comparison, we also need to account for finite-system-size effect, which can be done using the Hasimoto correction [1]:

$$D_{\mathrm{no-slip}} \sim D^{\infty} \left(1 - \frac{2.8373R}{L} + \frac{4\pi R^3}{3L^3} \right). \quad (1)$$

Fig. 2b demonstrates that the diffusion coefficient of a colloid with radius R=3.2 (corresponding to $\sim 2\,\mathrm{nm}$) is located approximately halfway between the slip and no-slip limits ($D_{\mathrm{slip}} = \frac{3}{2} D_{\mathrm{no-slip}}$). Using the Groot and Warren expression for the kinematic viscosity [2]: $\nu \approx 45 k_b T/(4\pi\gamma\rho r_c^3) + 2\pi\gamma\rho r_c^5/1575$, we find the dynamic viscosity μ =0.96 for the DPD fluid parameters used. We note that the Stokes radius of the colloid can vary slightly with the surface density of 'frozen' DPD particles.

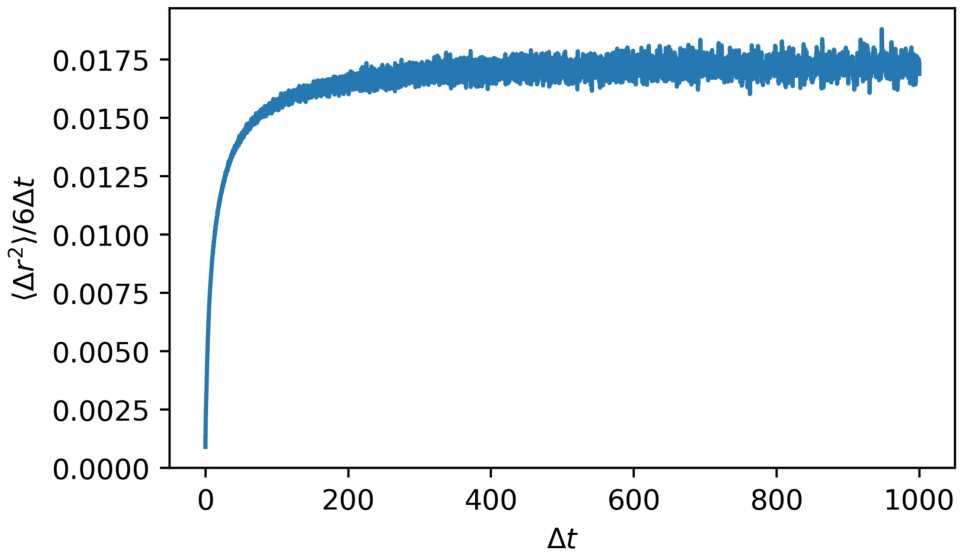

(a)

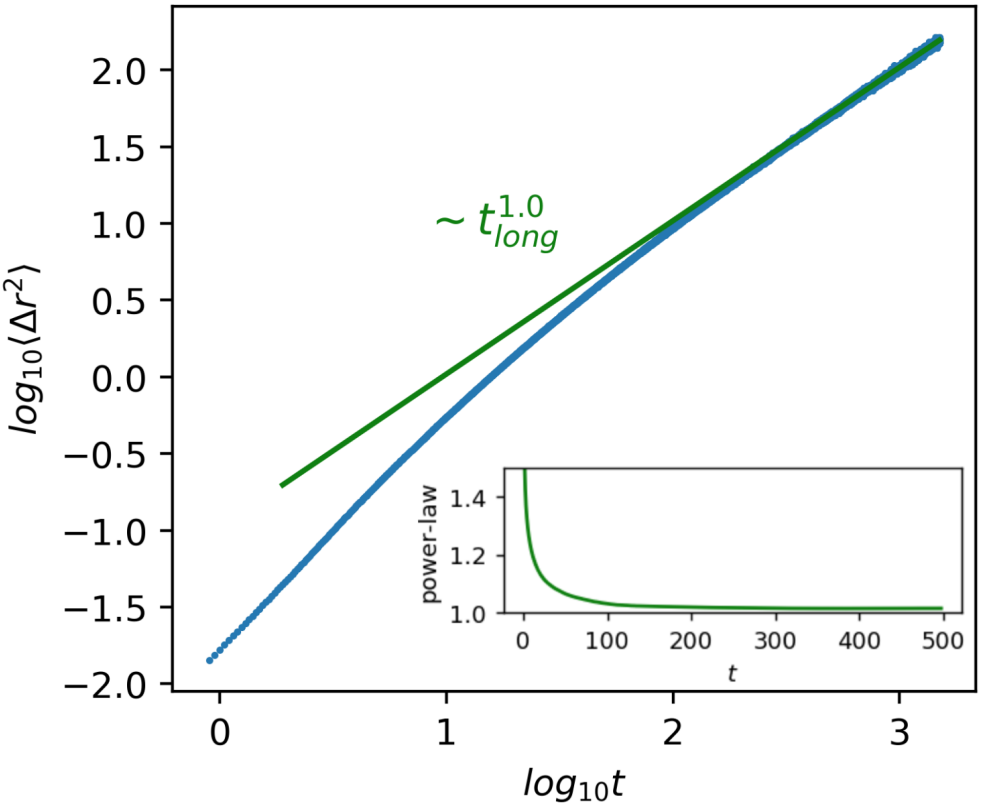

(b)

FIG. 1. (a) Example of the mean square displacement of a non-active colloid for the case where the ratio of the box length L to the colloidal radius R equals $L/R = 7.5$. (b) A Log-log plot of the colloidal mean-squared displacement versus time. As is clear from the figure, normal diffusive behavior (exponent = 1) is observed after some 200 time units. The inset shows the time dependence of the effective exponent, also showing the approach to the diffusive regime at long times.

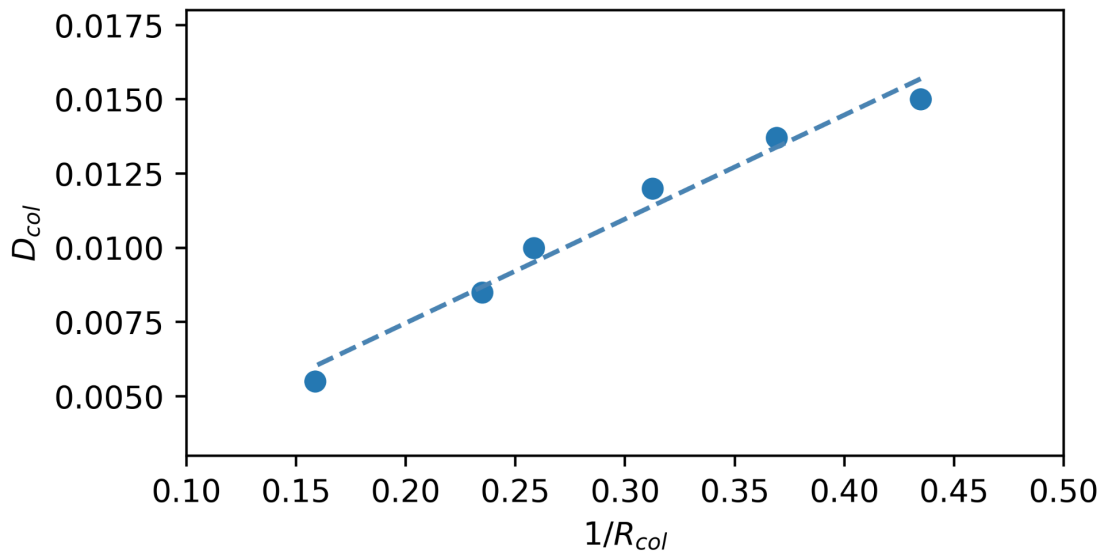

(a)

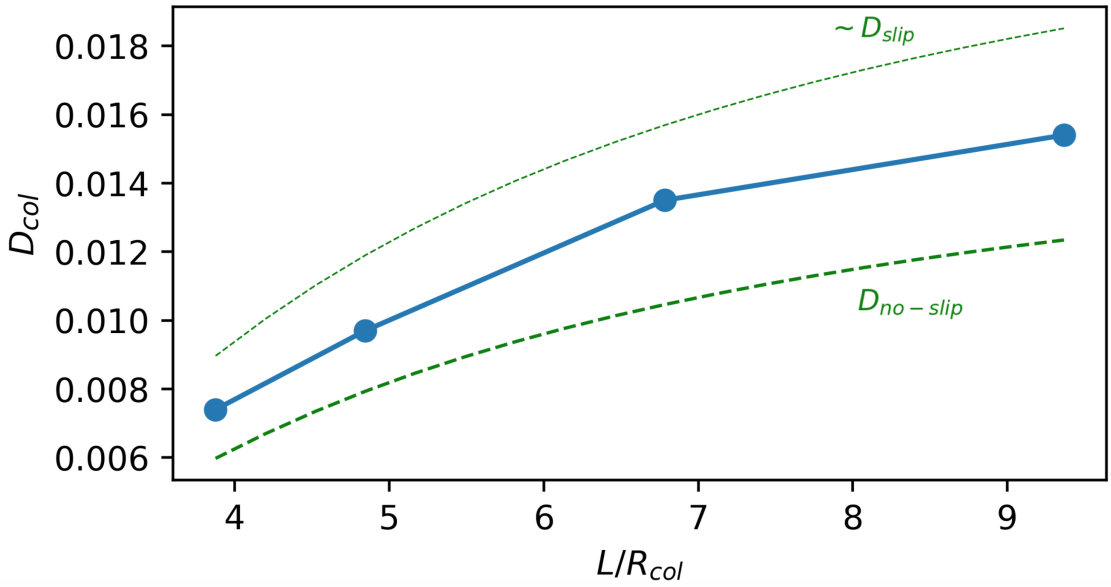

(b)

FIG. 2. (a) The diffusion coefficient of the colloid as function of the inverse of the colloid radius, $1/R$, whilst keeping the ratio $L/R = 7.5$. The curve indicates that $D \sim 1/R$, as expected from Stokes-Einstein relation. (b) The diffusion coefficient calculated for various ratios of box sizes to colloid radius (solid circles, solid line is a guide to the eye). The dash lines depict the non-slip (lower) and estimated slip (higher) limits. The colloid surface behaviour is approximately between slippery and non-slippery boundary conditions.

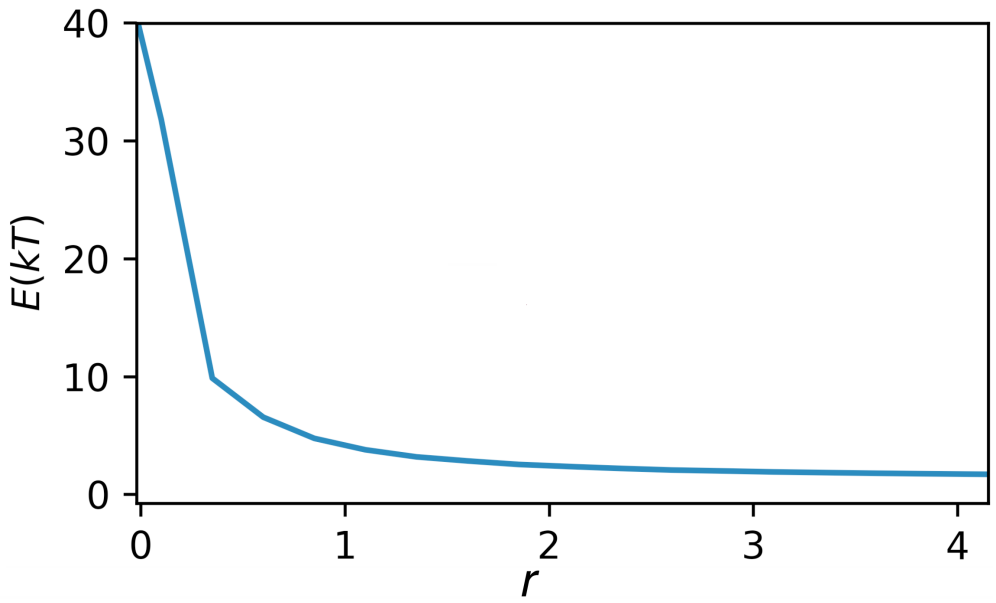

FIG. 3. Radial distance damping of the energy (kT) from a steady heat source.

Complementary Simulation: We test the effect of the thermostat in our model in order to show that thermal gradients can be neglected. We run a simulation of a DPD fluid in a box containing a small zone of high kinetic energy heat source (similar to the reaction heat produced in our study, $39.6kT$) in the center of a box, and we examine the decay of the averaged energy over the radial distance from the source. The averaged thermal decay is plotted in Fig. 3. It shows that the decay of temperature is in the order of r_c. The thermal gradient is minimal. Subsequently, it is reasonable to neglect contribution of thermophoresis as no thermal gradient occurs on the equatorial plane of the colloid.

Fig. 4 shows results of the colloid velocity as function of its inverse radius for the case of exothermic reaction at constant frequency. It shows that $|v_z|$ increases linearly with the inverse of the colloid radius, and proportional to the colloid friction, λ. This is indeed the case (within statistical error) for practical simulations over the range $1.36 \leq R \leq 4.6$ at constant f (where the ratio of the colloidal radius to the box diameter is kept approximately constant). The fact that $|v_z| \propto R^{-1}$ implies that $\langle \Delta p \rangle$ (the average momentum transferred to the colloid) is independent of the colloidal radius. Similarly, the inset of Fig. 4 shows that λv_z, *i.e.* the average momentum transfer per unit time, is effectively independent of R over this range of radii.

We examine the sensitivity of the momentum transfer mechanism to orientation of reac-

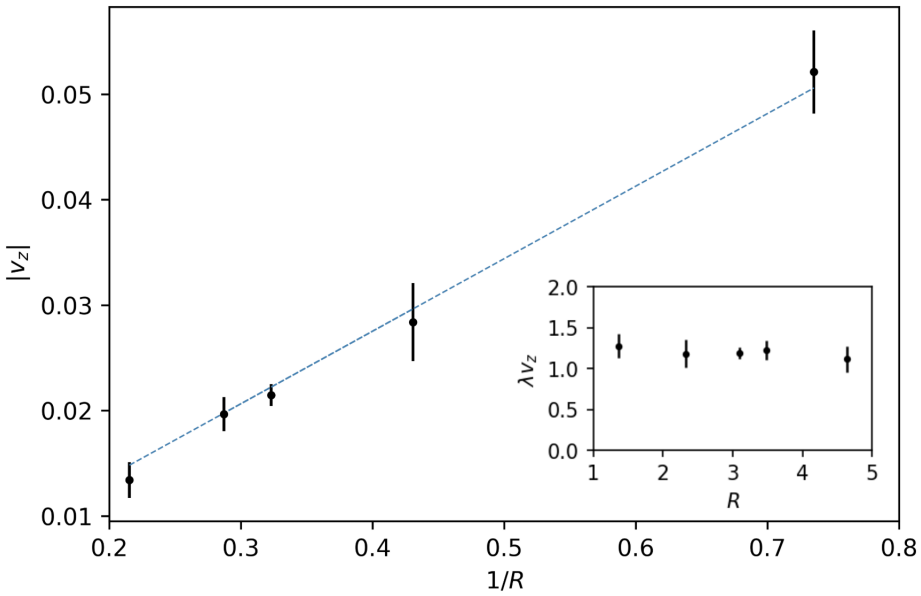

FIG. 4. Averaged velocity (Sample average and standard deviations of trajectories contain a total of 10^4 reactions in each data point) as function of the colloidal radius for the case of $f = 2$ (The fitted linear curve shown in blue dashed line). Inset: λv_z as a function of R.

tion. Fig 5 shows the average velocity of the colloid in the case of the momentum release from the reaction is constrained to xz or xy plane (and not distributed uniformly). The result shows that orientation of the initial motion of reaction products drastically affects the z drift velocity, which may even change its sign in the case of reaction parallel to the sphere.

[1] H. Hasimoto, On the periodic fundamental solutions of the stokes equations and their application to viscous flow past a cubic array of spheres, J. Fluid Mech. **5**, 317 (1959).

[2] R. D. Groot and P. B. Warren, Dissipative particle dynamics: Bridging the gap between atomistic and mesoscopic simulation, J. Chem. Phys. **107**, 4423 (1997).

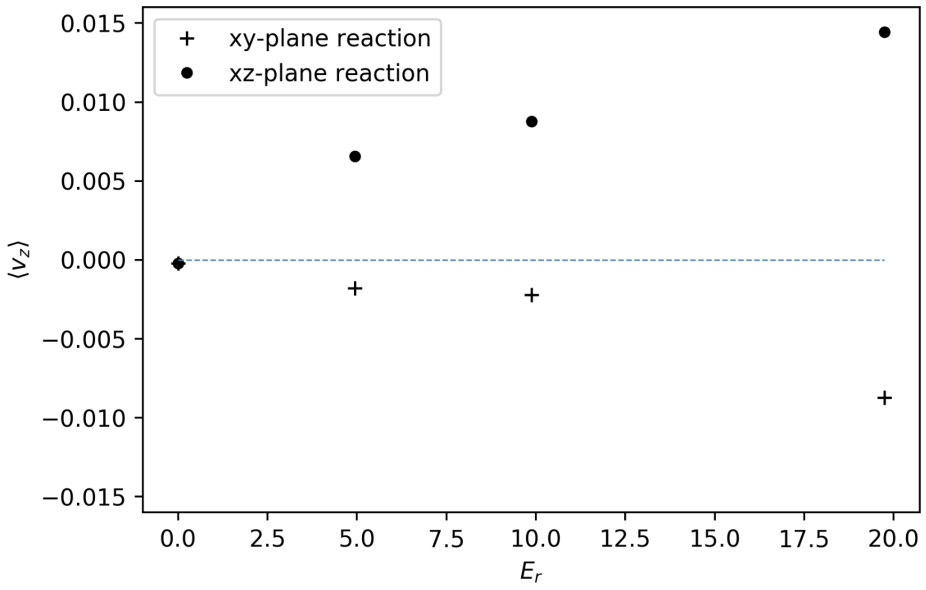

FIG. 5. Colloidal drift velocity as function of reaction energy release E_r for $R = 3.2$ and $f = 2$. The reaction products are constrained to lie in the xy (+) and xz (•) planes (parallel and perpendicular to the colloid reactive zone).